View metadata, citation and similar papers at core.ac.uk
brought to you by CORE
provided by Siberian Federal University Digital Repository

Corresponding author: V.V. Atuchin
Institute of Semiconductor Physics, Novosibirsk 630090, Russia
Phone: +7 (383) 3308889, Fax: +7 (383) 3332771
E-mail: atuchin@isp.nsc.ru

Triple molybdate scheelite-type upconversion phosphor $NaCaLa(MoO_4)_3:Er^{3+}/Yb^{3+}$: structural and spectroscopic properties

Chang Sung Lim[1], Aleksandr S. Aleksandrovsky[2,3], Maxim S. Molokeev[4,5], Aleksandr S. Oreshonkov[6,7], Denis A. Ikonnikov[7], Victor V. Atuchin[8,9,10]*

[1]Department of Advanced Materials Science & Engineering, Hanseo University, Seosan 356-706, Republic of Korea

[2]Laboratory of Coherent Optics, Kirensky Institute of Physics, SB RAS, Krasnoyarsk 660036, Russia

[3]Laboratory for Nonlinear Optics and Spectroscopy, Siberian Federal University, Krasnoyarsk 660079, Russia

[4]Laboratory of Crystal Physics, Kirensky Institute of Physics, SB RAS, Krasnoyarsk 660036, Russia

[5]Department of Physics, Far Eastern State Transport University, Khabarovsk 680021, Russia

[6]Laboratory of Molecular Spectroscopy, Kirensky Institute of Physics, SB RAS, Krasnoyarsk 660036, Russia

[7]Department of Photonics and Laser Technologies, Siberian Federal University, Krasnoyarsk 660079, Russia

[8]Laboratory of Optical Materials and Structures, Institute of Semiconductor Physics, SB RAS, Novosibirsk 630090, Russia

[9]Functional Electronics Laboratory, Tomsk State University, Tomsk 634050, Russia

[10]Laboratory of Semiconductor and Dielectric Materials, Novosibirsk State University, Novosibirsk 630090, Russia

Abstract

Triple molybdate $NaCaLa_{(1-x-y)}(MoO_4)_3:xEr^{3+},yYb3^+$ (x = y = 0, x = 0.05 and y = 0.45, x = 0.1 and y = 0.2, x = 0.2 and y = 0) phosphors were successfully synthesized by the microwave sol-gel method for the first time. Well-crystallized particles formed after heat-treatment at 900°C for 16 h showed a fine and homogeneous morphology with particle sizes of 2-3 μm. The structures were refined by Rietveld method in space group I41/a. The optical properties were examined comparatively using photoluminescence emission and Raman spectroscopy. Under the excitation at 980 nm, the $NaCaLa_{0.7}(MoO_4)_3:0.1Er^{3+},0.2Yb^{3+}$ and $NaCaLa_{0.5}(MoO_4)_3:0.05Er^{3+},0.45Yb^{3+}$ particles exhibited a strong 525-nm emission band, a weaker 550-nm emission band in the green region, and weak 655-nm, 490-nm and 410-nm emission bands in the red, blue and violet regions. The pump power dependence and Commission Internationale de L'Eclairage chromaticity of the upconversion emission intensity were evaluated in detail.

1. Introduction

For the recent years, the rare-earth doped oxide-based upconversion (UC) particles have become of extensive interest due to the stable luminescent properties and potential applications in photonic products such as lasers, three-dimensional displays, light-emitting devices, solar cells and biological luminescent imaging media [1-3]. Previously, scheelite-type binary molybdates were reported in terms of new structures, including structure-

modulation effects, promising spectroscopic characteristics and excellent upconversion (UC) photoluminescence properties [4-9]. In particular, the rare-earth binary $NaLn(MoO_4)_2$ (Ln = La^{3+}, Gd^{3+}, Y^{3+}) compounds possess the tetragonal phase with space group $I4_1/a$, and belong to the family of sheelite-type structure [10]. The trivalent rare-earth ions in the tetragonal phase can be partially substituted by laser-active Er^{3+}, Ho^{3+}, Tm^{3+} and Yb^{3+} ions. These ions are efficiently doped into the crystal lattice of the tetragonal binary molybdates due to the similar radii of the trivalent rare earth ions, which results in the excellent UC photoluminescence properties [4-9,11-14].

Among rare-earth ions, the Er^{3+} ion is suitable for the infrared to visible light conversion through the UC process due to its appropriate electronic energy level configuration. The Yb^{3+} ion, used as a sensitizer, can be dramatically excited by an incident light source energy. This energy is transferred to the activator from which radiation can be emitted. The Er^{3+} ion activator is the efficient luminescence center of the UC particles, while the sensitizer enhances the UC luminescence efficiency. The Er^{3+} and Yb^{3+} ions co-doping can remarkably enhance the UC efficiency for the shift from infrared to visible light due to the efficiency of the energy transfer from Yb^{3+} to Er^{3+} [15-17].

For preparation of the double molybdate $NaLn(MoO_4)_2$, several processes have been developed via specific preparation processes, including solid-state reactions [4,8,18-21], the sol-gel method [22,23], Czochralski growth [24-27], hydrothermal method [28-32], microwave assisted hydrothermal method [33] and pulse laser deposition [34]. Nevertheless, it is required to create new triple molybdate compounds for the observation of the UC photoluminescence in the materials and search for such features as the well-defined morphology and stable UC luminescent properties. However, up to now, the triple molybdates with general composition $NaRLn(MoO_4)_3$ (R = Ca^{2+}, Sr^{2+} and Ba^{2+}, while Ln is rare-earth elements) have not been reported on. As compared to the common technological

methods, microwave synthesis has its advantages of a very short reaction time, small-size particles, narrow particle size distribution, and high final polycrystalline samples purity [35,36]. The microwave heating is delivered to the material surface by radiant and/or convection heating and the heat energy is transferred to the bulk of the material via conduction [37-39]. It is an inexpensive method that provides high homogeneity powder products and it is easy to scale-up the process. Thus, the microwave method is considered as a viable alternative approach for the quick synthesis of high-quality luminescent materials. In this concept, this method is optimal for the synthesis of complex oxide compounds.

In the present study, the triple molybdate $NaCaLa_{(1-x-y)}(MoO_4)_3:xEr^{3+},yYb^{3+}$ (NCLM: xEr^{3+},yYb^{3+}) phosphors with the correct doping concentrations of Er^{3+} and Yb^{3+} (x = y = 0, x = 0.05 and y = 0.45, x = 0.1 and y = 0.2, x = 0.2 and y = 0) were successfully prepared by the microwave sol-gel method followed by heat treatment in the air. The synthesized particles were characterized by X-ray diffraction (XRD), scanning electron microscopy (SEM) and Energy-dispersive X-ray spectroscopy (EDS). The optical properties were examined comparatively using photoluminescence (PL) emission and Raman spectroscopy. The pump power dependence and Commission Internationale de L'Eclairage (CIE) chromaticity parameters of the UC emission were evaluated in detail.

2. Experimental methods

In this study, precise amounts of the raw materials were used by the products of Sigma-Aldrich (USA) for $Ca(NO_3)_2 \cdot 4H_2O$ (99 %), $Na_2MoO_4 \cdot 2H_2O$ (99%), $La(NO_3)_3 \cdot 6H_2O$ (99%), $Er(NO_3)_3 \cdot 5H_2O$ (99.9%), $Yb(NO_3)_3 \cdot 5H_2O$ (99.9%), Alfa Aesar (USA) for $(NH_4)_6Mo_7O_{24} \cdot 4H_2O$ (99%), Daejung Chemicals (Korea) for citric acid (99.5%), $NH_3 \cdot H_2O$ (A.R.), ethylene glycol (A.R.) and distilled water were used to prepare $NaCaLa(MoO_4)_3$, $NaCaLa_{0.8}(MoO_4)_3:0.2Er^{3+}$, $NaCaLa_{0.7}(MoO_4)_3:0.1Er_{3+},0.2Yb^{3+}$, and

$NaCaLa_{0.5}(MoO_4)_3$:0.05Er^{3+},0.45Yb^{3+} compositions. The reagents were taken in accordance with the nominal composition of the designed compounds. For the preparation of the compounds, initially 0.4 mol% $Ca(NO_3)_2$, 0.2 mol% $Na_2MoO_4 \cdot 2H_2O$ and 0.143 mol% $(NH_4)_6Mo_7O_{24} \cdot 4H_2O$ were dissolved in 20 mL of ethylene glycol and 80 mL of 5M $NH_3 \cdot H_2O$ under vigorous stirring and heating. Subsequently, 0.4 mol% (1-x-y)$La(NO_3)_3 \cdot 6H_2O$ with 0.4 mol% x$Er(NO_3)_3 \cdot 5H_2O$ and 0.4 mol% y$Yb(NO_3)_3 \cdot 5H_2O$ (x = 0.05 and y = 0.45, x = 0.1 and y = 0.2, x = 0.2 and y = 0) were dissolved in 100 mL of distilled water under vigorous stirring and heating. At this stage, the citric acid was employed with the molar ratio of citric acid to total metal ions of 2:1. Then, the two kind of transparent solutions were co-mixed together with the vigorous stirring under heating at 80-100°C. Finally, the mixed solutions were appeared as highly transparent and treated by the adjusting to pH = 7-8 using the addition of citric acid or $NH_3 \cdot H_2O$. The co-mixed and adjusted solutions were moved into an oven for microwave irradiation. The microwave operations for 30 min were conducted by the precise controlling. The frequency was 2.45 GHz and the maximum output-power was 1250 W. After the microwave process, the samples were treated in ultrasonicator for 10 min, and move into a dry oven. The drying conditions were at 120°C and dried gels as a black color were obtained. For the crystallization of the compounds, the black dried gels were heat-treated at 900°C for 16 h. Finally, the white pure $NaCaLa(MoO_4)_3$ and pink particles for the Er/Yb-doped compositions were obtained. The chemical compositions of the final powder products were confirmed by EDS measurements.

The powder diffraction data of the synthesized particles for Rietveld analysis were collected over the range of 2θ = 5-90° at room temperature with a D/MAX 2200 (Rigaku, Japan) diffractometer (Cu-Kα radiation, θ-2θ geometry). The step size of 2θ was 0.02°, and the counting time was 5 s per step. The microstructure and surface morphology of the synthesized particles were observed using SEM (JSM-5600, JEOL, Japan). The PL spectra

were recorded using a spectrophotometer (Perkin Elmer LS55, UK) at room temperature. Pump power dependence of the UC emission intensity was measured at working power from 20 to 110 mW levels. Raman spectra measurements were performed using a LabRam Aramis (Horiba Jobin-Yvon, France) with the spectral resolution of 2 cm^{-1}. The 514.5-nm line of an Ar ion laser was used as an excitation source; the power on the samples was kept at the 0.5 mW level to avoid the sample decomposition.

3. Results and discussion

The XRD patterns recorded from the synthesized molybdates are shown in Figures 1 and 1S-3S. In general, the patterns of solutions NCLM:xEr^{3+},yYb^{3+} are similar. The difference profile plot of NCLM is shown in Fig. 1. The difference profile plots of NCLM:xEr^{3+},yYb^{3} are very similar to that of NCLM, as it is evident from the comparison of Figs. 1 and 1S-3S. $^{+}$

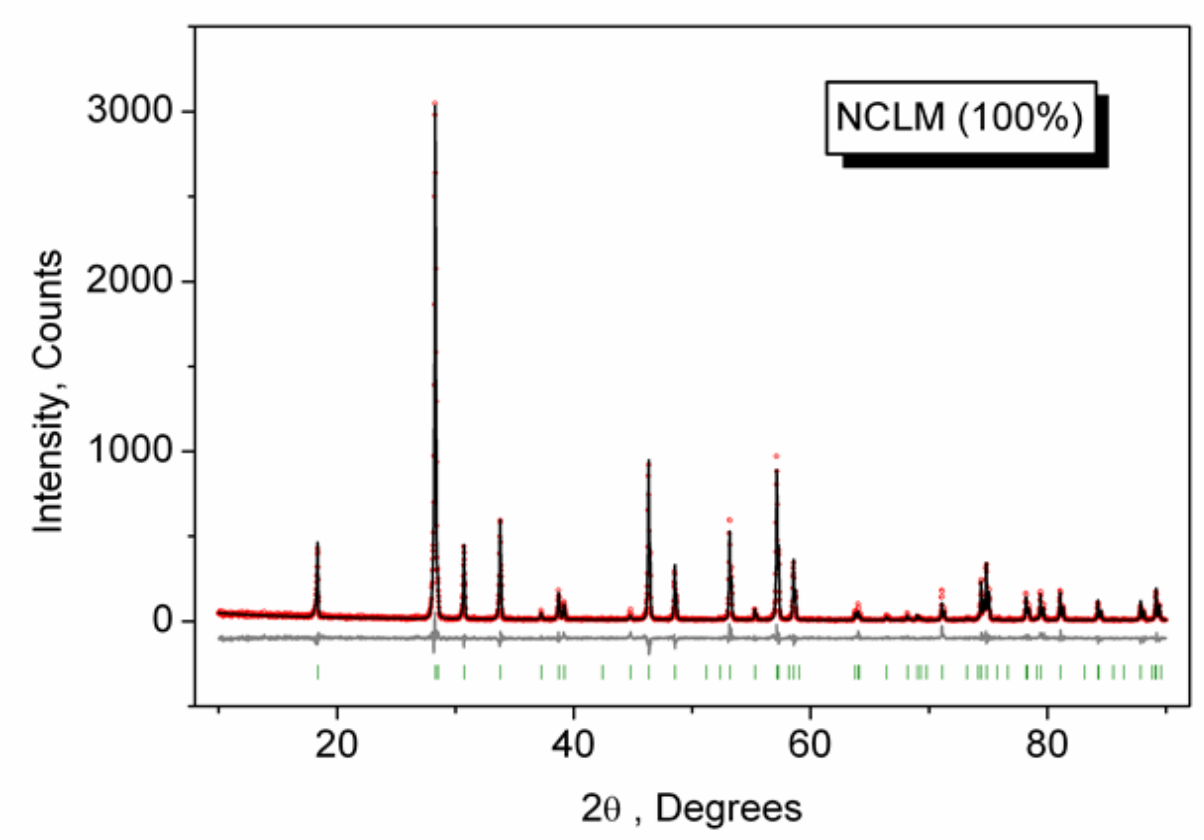

Fig. 1. The difference Rietveld plot of NCLM.

Rietveld refinement was performed using a TOPAS 4.2 package [40]. All diffraction peaks were indexed by the tetragonal unit cell in space group $I4_1/a$ with parameters close to those of $CaMoO_4$ [41] and $Na_{0.5}La_{0.5}MoO_4$ [42]. Therefore, these crystal structures were taken as a starting model for the Rietveld refinement. The site of Ca or (Na/La) ion was taken as occupied by Ca, Na, La, Er, Yb ions at fixed occupations according to the nominal compositions. The refinement was stable and gave low *R*-factors (Table 1, Figs. 1 and 1S-3S). The obtained atom coordinates and the main bond lengths can be found in Tables 1S and

Table 1. Main parameters of processing and refinement of the NCLM:xEr^{3+},yYb^{3+} samples

Compound	NCLM	NCLM:0.2Er^{3+}	NCLM:0.1Er^{3+},0.2Yb^{3+}	NCLM:0.05Er^{3+},0.45Yb^{3+}
x	0	0.2	0.1	0.05
y	0	0	0.2	0.45
Sp. gr.	$I4_1/a$	$I4_1/a$	$I4_1/a$	$I4_1/a$
a, Å	5.2991 (1)	5.2806 (2)	5.2675 (1)	5.2421 (1)
c, Å	11.6223 (3)	11.5726 (3)	11.5377 (3)	11.4678 (2)
V, $Å^3$	326.37 (2)	322.70 (1)	320.13 (2)	315.17 (1)
Z	4	4	4	4
2θ-interval, deg.	5-90	5-90	5-90	5-90
No. of reflections	70	70	70	70
No. of refined parameters	7	7	7	7
R_{wp}, %	19.46	16.75	15.65	15.06
R_p, %	13.39	11.30	10.31	9.97
R_{exp}, %	16.22	14.87	13.61	13.49
χ^2	1.20	1.13	1.15	1.12
R_B, %	5.29	3.15	2.09	1.65

2S, respectively. In the compounds under consideration, Z = 4 and, from structural point of view [43], total chemical formula calculated by summing all elements in unit cell $Na_{4/3}Ca_{4/3}La_{4(1-x-y)/3}(MoO_4)_4$:$4x/3Er^{3+}$,$4y/3Yb^{3+}$ can be generalized as $Na_{1/3}Ca_{1/3}La_{(1-x-y)/3}MoO_4$:$(x/3)Er^{3+}$,$(y/3)Yb^{3+}$ that clearly emphasizes the relation of the solid solutions to the $CaMoO_4$ structural family [41]. As an example, the structure of NCLM is shown in Fig. 2.

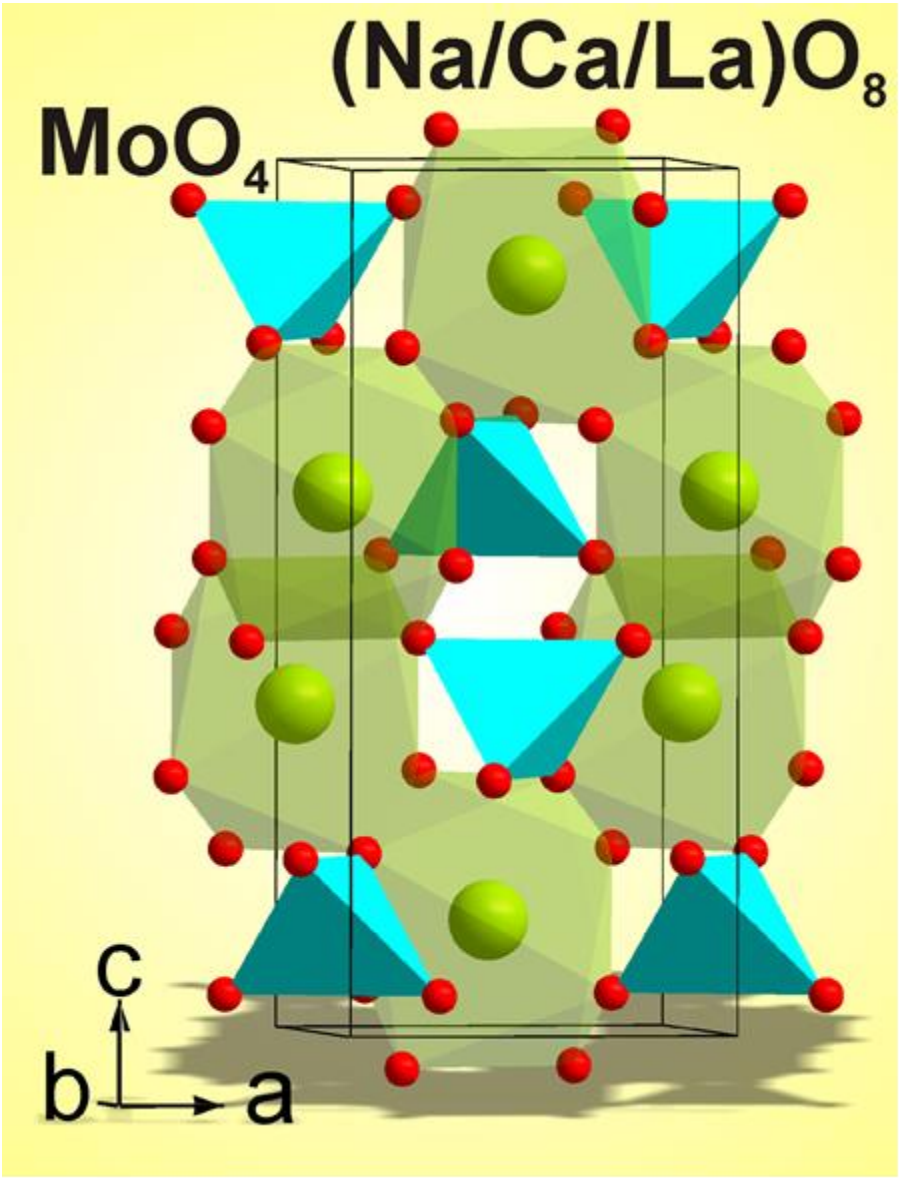

Fig. 2. The crystal structure of NCLM. The unit cell is outlined.

The linear cell volume increase on the averaged increase of ion radii IR(Na/Ca/La/Er/Yb), as shown in Fig. 3, proves the chemical compositions of the synthesized samples [44]. On the base of the structural results, it can be reasonably supposed that different triple molybdates with general composition $NaRLn(MoO_4)_3$ should crystallize in tetragonal structures close to that of $CaMoO_4$ and the general formula should be rewritten as $Na_{1/3}R_{1/3}Ln_{1/3}MoO_4$. Further details of the crystal structure may be obtained from Fachinformationszentrum Karlsruhe, 76344 Eggenstein-Leopoldshafen, Germany (fax: (+49)7247-808-666; E-mail: crystdata@fiz-karlsruhe.de; http://www.fiz-karlsruhe.de/request_for_deposited_data.html on quoting the deposition numbers: CSD-431015-431018.

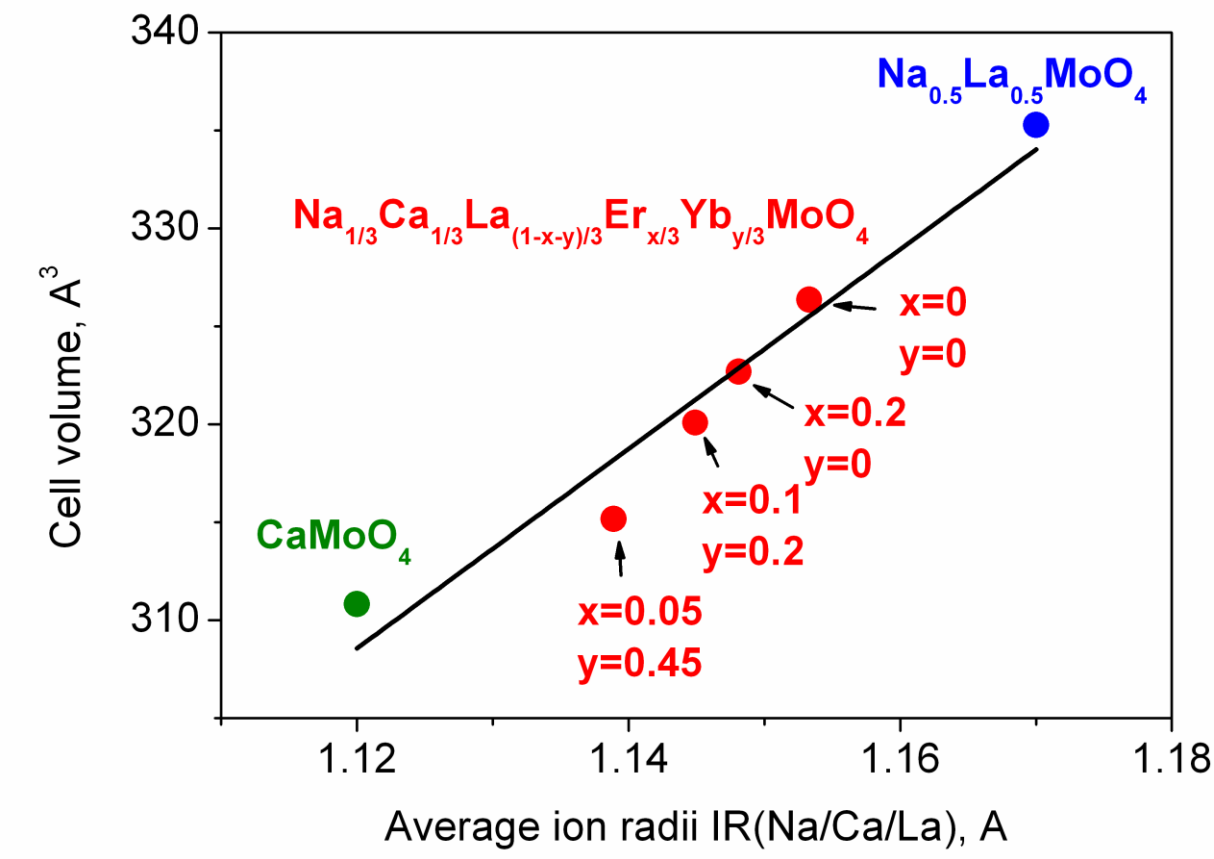

Fig. 3. Cell volume per averaged ion radii IR(Na/Ca/La/Er/Yb) of $CaMoO_4$ (green) [41], NCLM: $x\mathrm{Er}^{3+}$,$y\mathrm{Yb}^{3+}$ (red) and $Na_{0.5}La_{0.5}MoO_4$ (blue) [42] compounds.

Thus, the post heat-treatment plays an important role in the molybdate gel crystallization. To reach a high-quality crystalline state, the samples need to be heat treated at 900°C for 16 h. It should be pointed that this temperature is optimal for molybdate treatment in the air and, earlier, other simple and complex molybdates were formed at close temperatures [6,7,9,37-39,45-47]. Besides excellent crystallinity, the selected synthesis route provides very uniform particle morphology. The SEM images of the synthesized (a) NCLM:0.2Er^{3+} and (b) NCLM:0.05Er^{3+},0.45Yb^{3+} particles are shown in Fig. 4. The as-synthesized samples are well formed with a fine and homogeneous morphology and the particle size of 2-3 μm. The samples have no discrepancy in the aspect of morphological feature, and closely agglomerated particles were induced by the active grain interdiffusion [48-50]. It should be noted that the doping concentrations of Er^{3+} and Yb^{3+} have no effects for the particle morphology. The recorded EDS patterns and quantitative compositions of the NCLM:0.1Er^{3+},0.2Yb^{3+} sample are shown in Fig. 4S and Table 3S. Only constituent elements are found in the samples and the quantitative compositions are in good relation with nominal compositions. Thus, the microwave sol-gel method of the triple molybdate preparation provides the energy uniformly over the material bulk, and the fine particles with controlled morphology can be fabricated for a short time. The method is an inexpensive way to fabricate highly homogeneous powder products with an easy scale-up and it is a viable alternative for the rapid synthesis of UC particles. This suggests that the microwave sol-gel route is suitable for the creation of homogeneous NCLM:xEr^{3+},yYb^{3+} crystallites and it can be successfully applied for other molybdates from this crystal family.

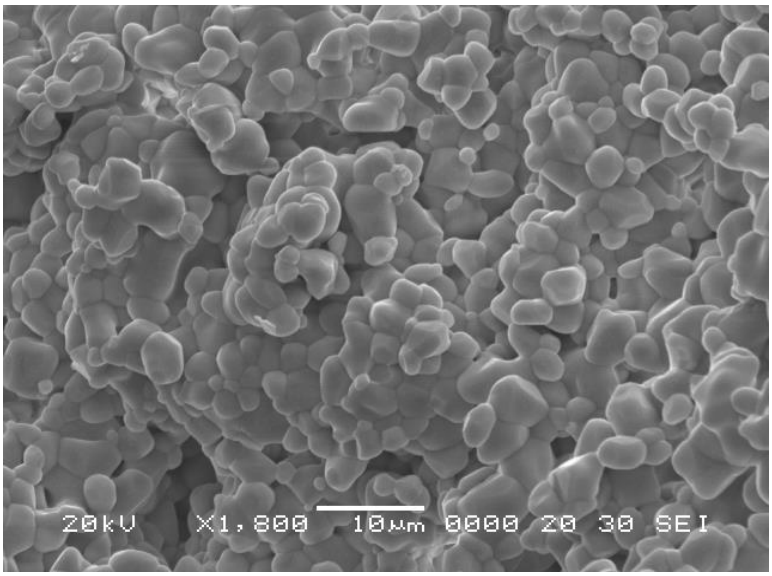

(a)

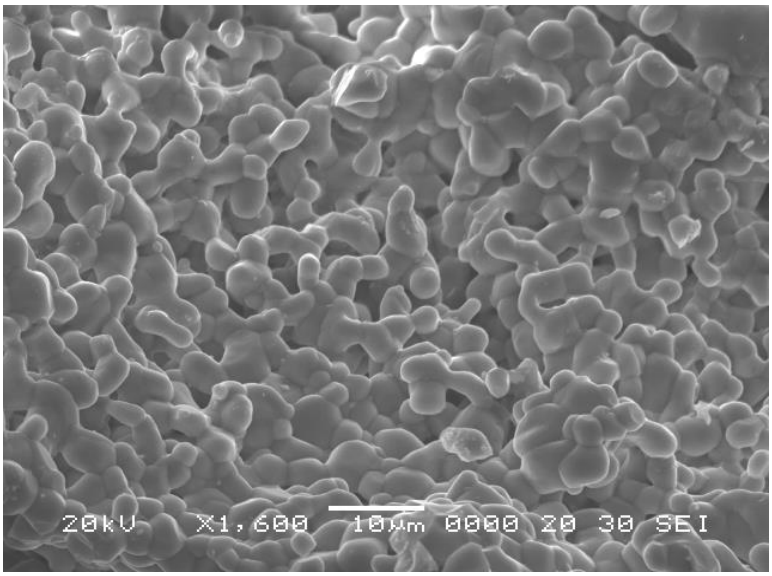

(b)

Fig. 4. Scanning electron microscopy images of the synthesized (a) NCLM:0.2Er^{3+} and (b) NCLM:0.05Er^{3+},0.45Yb^{3+} particles.

The UC photoluminescence emission spectra of the as-prepared NCLM, NCLM:0.2Er^{3+}, NCLM:0.1Er^{3+},0.2Yb^{3+} and NCLM:0.05Er^{3+},0.45Yb^{3+} particles excited under 980 nm at room temperature are shown in Fig. 5. The UC NCLM:0.1Er^{3+},0.2Yb^{3+} and NCLM:0.05Er^{3+},0.45Yb^{3+} particles exhibited a strong 525-nm emission band, a weaker 550-

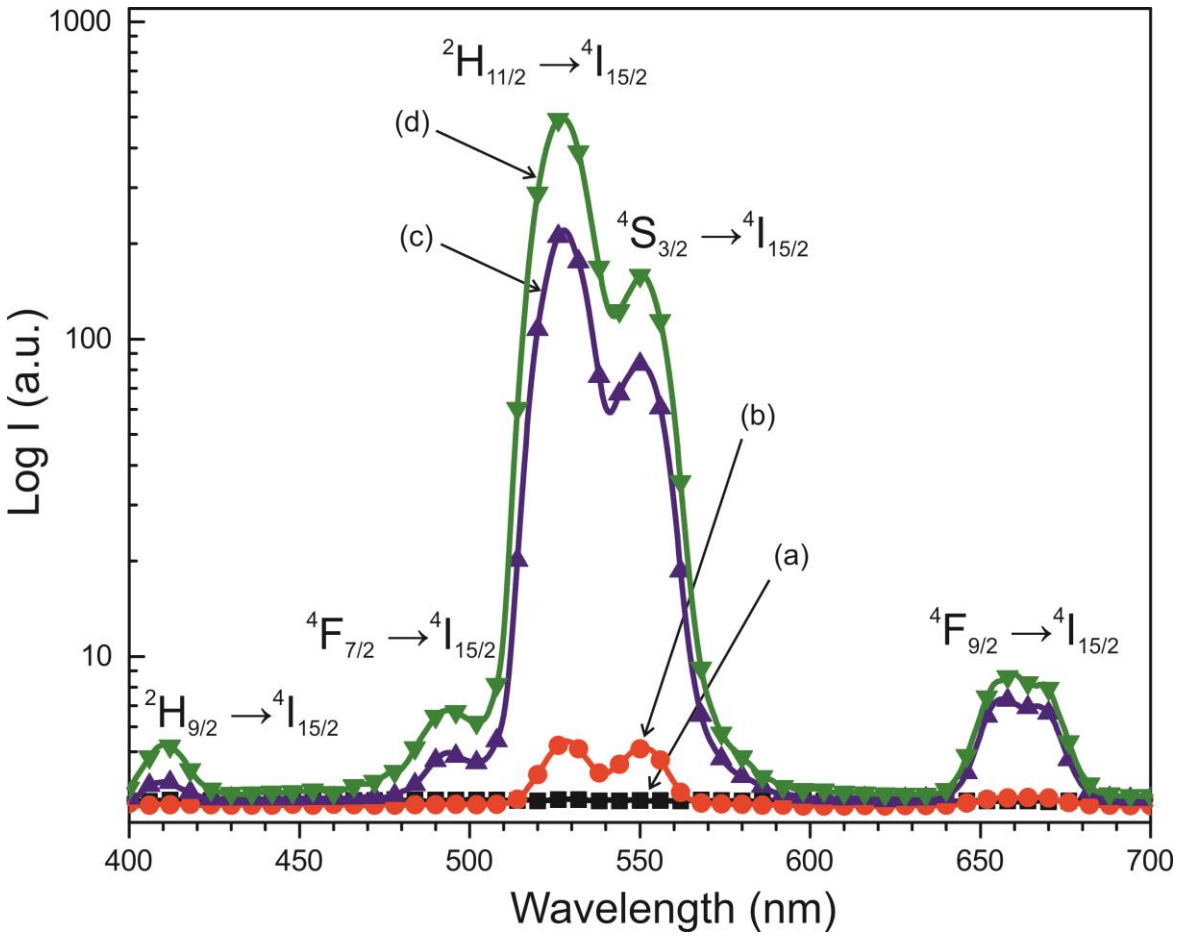

Fig. 5. The upconversion photoluminescence emission spectra of (a) NCLM, (b) NCLM:0.2Er^{3+}, (c) NCLM:0.1Er^{3+},0.2Yb^{3+}, and (d) NCLM:0.05Er^{3+},0.45Yb^{3+} particles excited under 980 nm at room temperature. Logarithmic scale is used along vertical axis.

nm emission band in the green region and three very weak emission bands: at 655 nm in the red region, at 490 nm in the blue, and at 410 nm in the violet region. The strong 525-nm emission band and the weak 550-nm emission band in the green region correspond to the $^2H_{11/2} \rightarrow {}^4I_{15/2}$ and $^4S_{3/2} \rightarrow {}^4I_{15/2}$ transitions, respectively, while the very weak emission 655-nm band in the red region corresponds to the $^4F_{9/2} \rightarrow {}^4I_{15/2}$ transition. Another very weak band at 410 nm is due to $^2H_{9/2} \rightarrow {}^4I_{15/2}$ transition, while 490 nm peak is due to $^4F_{9/2} \rightarrow {}^4I_{15/2}$ transition. It must be noted that in the sample d) the shortest-wavelength band at 410 nm is only two times smaller than the red one, despite the fact that three-stage process is necessary

to excite $^2H_{9/2}$ level. The mechanism of excitation of this level might be the energy transfer from Yb excited state to Er $^4F_{9/2}$ level, since energy difference between $^4F_{9/2}$ and $^2H_{9/2}$ is close to the energy of excited Yb ion. However, since $^4F_{9/2}$ population is likely to be low, the most probable excitation channel is the population of a pair of high-lying levels $^4G_{9/2}$ and $^2K_{15/2}$ from well-populated $^4S_{3/2}$ level through the energy transfer from Yb ion, with the subsequent decay of these high-lying levels to $^2H_{9/2}$ one.

The UC intensities of NCLM were not detected. The UC intensities of NCLM:0.2Er^{3+} are well above the detection limit; however, they are one or two orders of magnitude smaller than those of the Yb-doped samples, and, hence, the UC luminescence for an Er-doped sample is not well seen in Fig. 5. The UC luminescence is observed from all levels: $^2H_{11/2}$, $^4S_{3/2}$ and even from $^4F_{9/2}$. The intensity ratio of green and red lines is 1.4 for sample (b), 30 for sample (c) and 56 for sample (d). At the same time, the ratio of UC green band peak values for samples (d) and (b) is 92. The latter effect admits that the absorption coefficient of erbium at 980 nm is much smaller than that of ytterbium in the matrix under study. The green-to-red ratio variation with the ytterbium content increase is rather common and it was observed earlier for several hosts [15-17,37-39].

The Er^{3+} ion activator is the luminescence center of these UC particles and sensitizer Yb^{3+} effectively enhances the UC luminescence intensity because of the efficient energy transfer from Yb^{3+} to Er^{3+}. The concentration quenching effect can be explained by the energy transfer between the nearest Er^{3+} and Yb^{3+} ions. With increasing Er^{3+} and Yb^{3+} ion concentrations, the distance between Er^{3+} and Yb^{3+} ions decrease, which can promote a non-radiative energy transfer, such as an exchange interaction or multipole-multipole interactions [51]. As shown in Fig. 5, the higher intensity of (d) NCLM:0.05Er^{3+},0.45Yb^{3+} is caused by the ratio of Yb^{3+}:Er^{3+} = 9:1, while the lower intensity of (c) NCLM:0.1Er^{3+},0.2Yb^{3+} is caused by the ratio of Yb^{3+}:Er^{3+} = 2:1. Thus, the preferable Yb^{3+}:Er^{3+} = 9:1 ratio is induced by the

concentration quenching effect of Er^{3+} ions. Therefore, the higher content of the Yb^{3+} ions used as a sensitizer and a lower content of the Er^{3+} ions close to the preferable ratio of Yb^{3+}:Er^{3+} = 9:1 can remarkably enhance the UC luminescence through the efficient energy transfer. The ratio of the $^2H_{11/2} \rightarrow {}^4I_{15/2}$ and $^4S_{3/2} \rightarrow {}^4I_{15/2}$ transitions intensities may be influenced not only by the change in radiation probabilities from starting levels, but also by the probabilities of the non-radiative relaxation from the UC-populated $^4F_{7/2}$ level. Because the life time of the $^4F_{7/2}$ level is comparatively short, the excited Er^{3+} ions decay non-radiatively to the $^2H_{11/2}$ level with a higher probability, as compared to the $^4S_{3/2}$ level, in the case of the NCLM host matrix.

The logarithmic scale dependences of the UC emission intensities at 525, 550 and 655 nm on the working pump power over the range of 20 to 110 mW in the NCLM:0.05Er^{3+},0.45Yb^{3+} sample are shown in Fig. 6. In the UC process, UC emission intensity *I* is proportional to the slope value *n* of the irradiation pumping power *P*. Maximum value of n is the number of pumping photons required to reach the starting energy level in the UC ion and produce UC emission [52]:

$$I \propto P^n \quad (1)$$

$$\mathrm{Ln}I \propto n\mathrm{Ln}P \quad (2)$$

The slopes n = 1.70 and 1.68 for green emission at 525 and 550 nm, and n = 1.56 for red emission at 655 nm, respectively, are evident from Fig. 5. These results exhibit that the UC mechanism of the green and red emissions can be explained by a two-photon UC process in the Er^{3+}/Yb^{3+} co-doped phosphors [53-55].

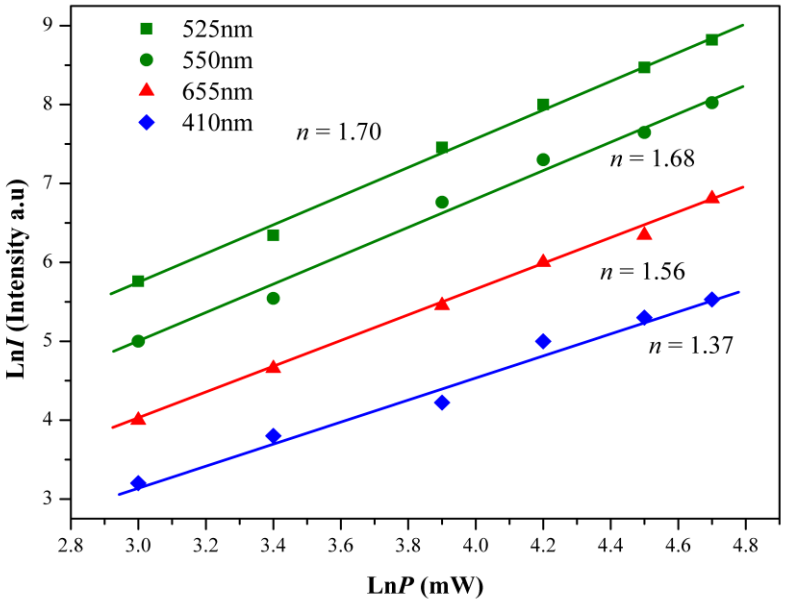

Fig. 6. The logarithmic scale dependence of the upconversion emission intensity on the pump power in the range from 20 to 110 mW at 525, 550, 655 and 410 nm in the NCLM:0.05Er^{3+},0.45Yb^{3+} sample.

Based on the results of the analysis of pump power dependence, the schematic energy level diagrams of Er^{3+} ions (activator) and Yb^{3+} ions (sensitizer) in the NCLM:xEr^{3+},yYb^{3+} samples and the UC mechanisms, accounting for the green and red emissions excited by the 980 nm laser wavelength, are shown in Fig. 7. The UC emissions are generated via multiple processes of ground state absorption (GSA), energy transfer upconversion (ETU), excited state absorption (ESA) and cross relaxation (CR). Under the excitation at 980 nm, the Er^{3+} and Yb^{3+} ions are initially excited from the ground state to the excited state through the ground state absorptions (GSA) process (Er^{3+}: $^4I_{15/2} \rightarrow {}^4I_{11/2}$, Yb^{3+}: $^2F_{7/2} \rightarrow {}^2F_{5/2}$) and ETU processes of $^4I_{15/2}$ (Er^{3+}) + $^2F_{5/2}$ (Yb^{3+}) → $^4I_{11/2}$ (Er^{3+}) + $^2F_{7/2}$ (Yb^{3+}) which are responsible for

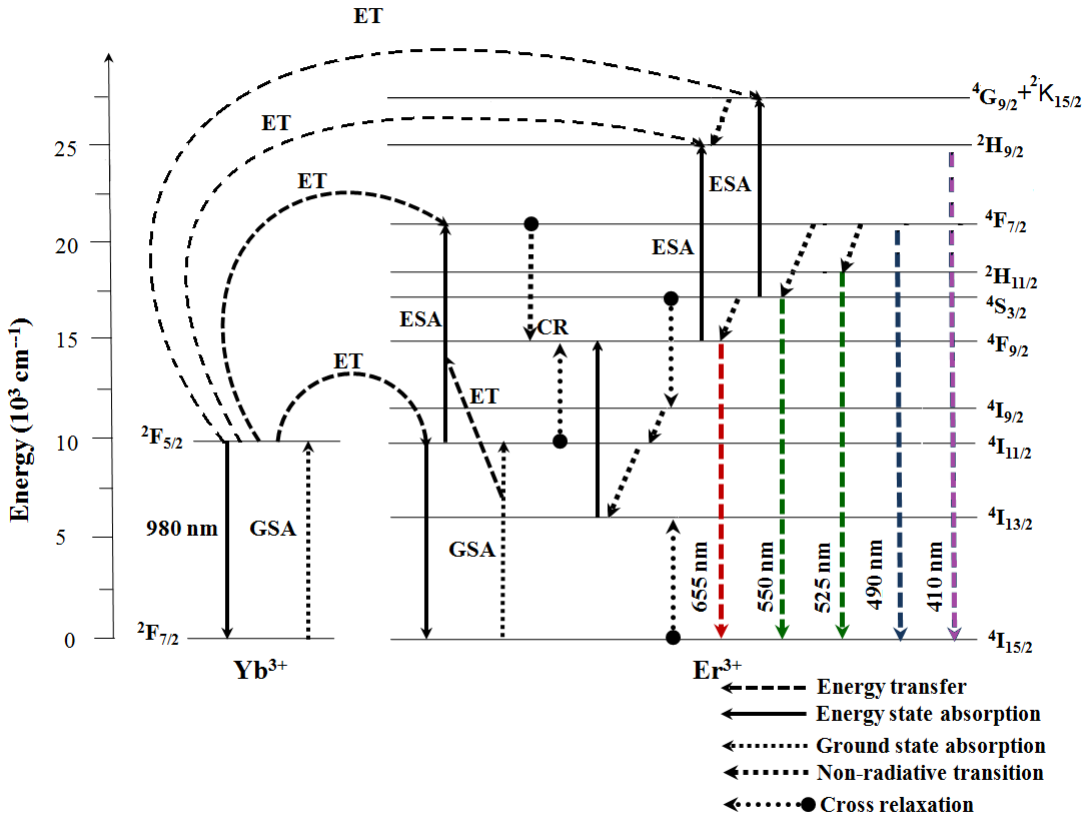

Fig. 7. The schematic energy level diagrams of Yb^{3+} (sensitizer) and Er^{3+} ions (activator) ions in the NCLM:$x$$Er^{3+}$,$y$$Yb^{3+}$ system and the upconversion mechanisms of the green and red emissions under 980 nm laser excitation.

the population at the $^4I_{11/2}$ level in the Er^{3+} ion. For the green emissions, the energy transition from the $^4I_{11/2}$ level to the $^4F_{7/2}$ level of Er^{3+} is involved into the three possible processes [53-55]; (1) ESA: $^4I_{11/2}$ (Er^{3+}) + a photon (980 nm) → $^4F_{7/2}$, (2) ETU: $^2I_{11/2}$ (Er^{3+}) + $^2F_{5/2}$ (Yb^{3+}) → $^4F_{7/2}$ (Er^{3+}) + $^2F_{7/2}$ (Yb^{3+}) and (3) ETU: $^4I_{11/2}$ (Er^{3+}) + $^4I_{11/2}$ (Er^{3+}) → $^4F_{7/2}$ (Er^{3+}) + $^4I_{15/2}$ (Er^{3+}). These three possible processes can populate the $^4F_{7/2}$ level from the $^4I_{11/2}$ level in Er^{3+} and, then, the $^4F_{7/2}$ level relaxes rapidly and non-radiatively to the next lower $^2H_{11/2}$ and $^4S_{3/2}$ levels in Er^{3+} because of the short lifetime of the $^4F_{7/2}$ level. As a result, the radiative transitions of $^2H_{11/2}$ → $^4I_{15/2}$ and $^4S_{3/2}$ → $^4I_{15/2}$ processes can generate the green emission at 525 and 550 nm.

Strong suppression of red UC luminescence in the host under study is similar to the effect in the earlier studied $CaGd_2(MoO_4)_4$:Er,Yb and $CaGd_2(WO_4)_4$:Er,Yb systems and differentiates this host class from a number of others. For the red emission, the $^4F_{9/2}$ level population is generated by non-radiative relaxation either 1) from the $^4S_{3/2}$ to the $^4F_{9/2}$ level or 2) from $I_{11/2}$ to $I_{13/2}$, then pumping to $^4F_{9/2}$, as well as cross relaxation (CR) via either 3) $^4F_{7/2} + {}^4I_{11/2} \rightarrow {}^4F_{9/2} + {}^4F_{9/2}$ transition [51-53] or 4) $^4S_{3/2} + {}^4I_{15/2} = {}^4I_{9/2} + {}^4I_{13/2}$, then pumping to $^4F_{9/2}$ [56]. Finally, the $^4F_{9/2}$ level relaxes radiatively to the ground state at the $^4I_{15/2}$ level, and releases the red emission at 655 nm [37-39]. The radiation-free transitions 1) and 2) must not strongly vary from one oxide host to another, and, then. they cannot provide such significant difference between the red and green luminescence in the selected group of hosts. Consequently, processes 1) and 2) must be deduced to play a negligible role in host class under study. So, intense red luminescence at Er/Yb ratio 3/8 is most likely, due to one of the mentioned cross-relaxation channels [54]. The 3) $^4F_{7/2} + {}^4I_{11/2} = {}^4F_{9/2} + {}^4F_{9/2}$ cross-relaxation will be very weak since $^4F_{7/2}$ has a comparatively short life time and its radiationless depopulation to $^4S_{3/2}$ and $^2H_{11/2}$ levels is rather fast, which may explain the weak red luminescence in our host. For the 4) population channel, weak red UCL is explainable by the suggestion that, in our host, detuning between the energy of $^4S_{3/2}$ state and the sum of energies of $^4I_{9/2}$ and $^4I_{13/2}$ states is not so favorable [54]. Moreover, as Yb^{3+} concentration increases, the green emission dramatically increases, compared to the red emission. The strong 525-nm and 550-nm emission lines in the green region, as shown in Figure 5, are assigned to the $^2H_{11/2} \rightarrow {}^4I_{15/2}$ and $^4S_{3/2} \rightarrow {}^4I_{15/2}$ transitions of the Er^{3+} ions, respectively, while the weak 655-nm emission band in the red region is assigned to the $^4F_{9/2} \rightarrow {}^4I_{15/2}$ transition.

The calculated chromaticity coordinates calculated for (a) NCLM:$0.1Er^{3+}$,$0.2Yb^{3+}$ and (b) NCLM:$0.05Er^{3+}$,$0.45Yb^{3+}$ particles and the related CIE chromaticity diagram are shown in Fig. 8. The legend in Figure 8(B) shows the chromaticity points for the samples (a) and (b).

When the Er^{3+}/Yb^{3+} concentration ratio is varied, the chromaticity coordinate values (x, y) are changed. As shown in Fig. 8(A), the calculated chromaticity coordinates x = 0.227 and y = 0.686 for (a) NCLM:$0.1Er^{3+}$,$0.2Yb^{3+}$ and x = 0.206 and y = 0.727 for (b) NCLM:$0.05Er^{3+}$,$0.45Yb^{3+}$ correspond to the yellowish-green sector in the CIE diagram.

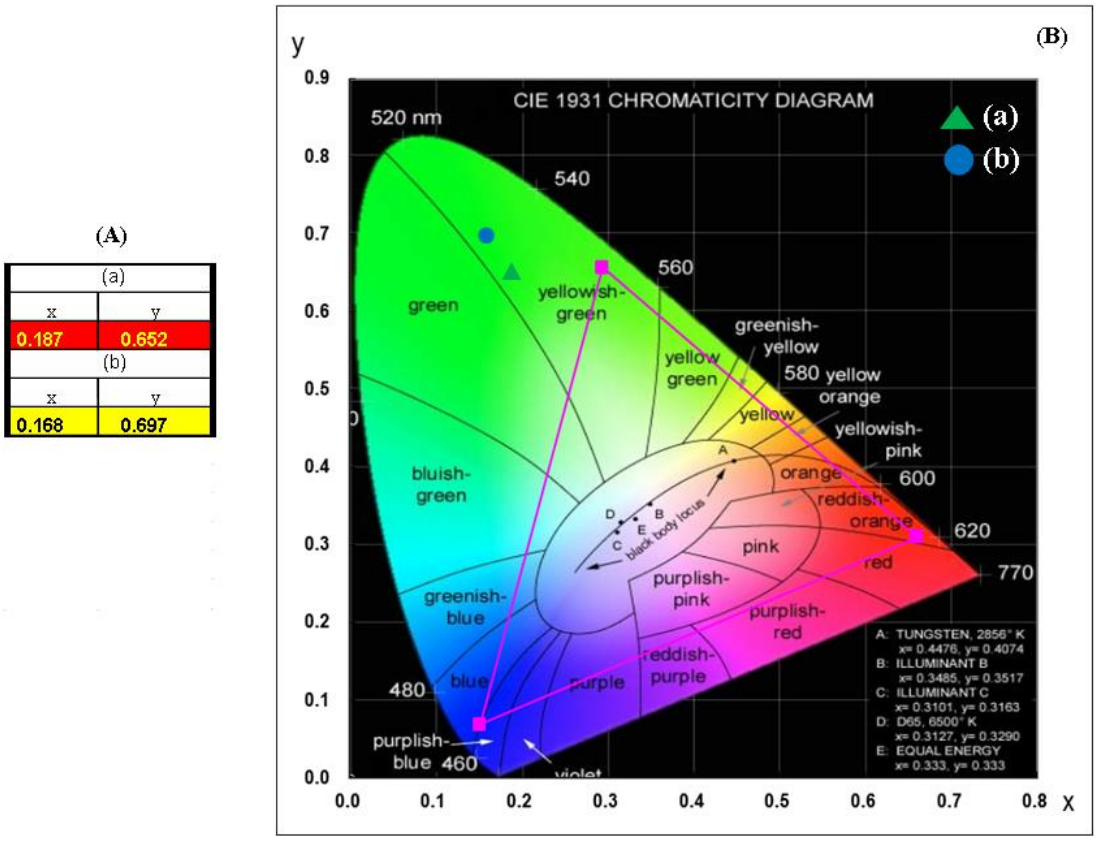

Fig. 8. (A) Calculated chromaticity coordinates (x, y) values and the (B) CIE chromaticity diagram for the NCLM:xEr^{3+},yYb^{3+} phosphors. The emission points for the sample (a) NCLM:$0.1Er^{3+}$,$0.2Yb^{3+}$, and (b) NCLM:$0.05Er^{3+}$,$0.45Yb^{3+}$ particles are shown in the inset.

The Raman spectra of the synthesized pure NCLM, NCLM:$0.2Er^{3+}$, NCLM:$0.1Er^{3+}$,$0.2Yb^{3+}$ and NCLM:$0.05Er^{3+}$,$0.45Yb^{3+}$ particles are shown in Fig. 9. As to pure NCLM, the well-resolved sharp peaks clearly indicate a high crystalline state of the

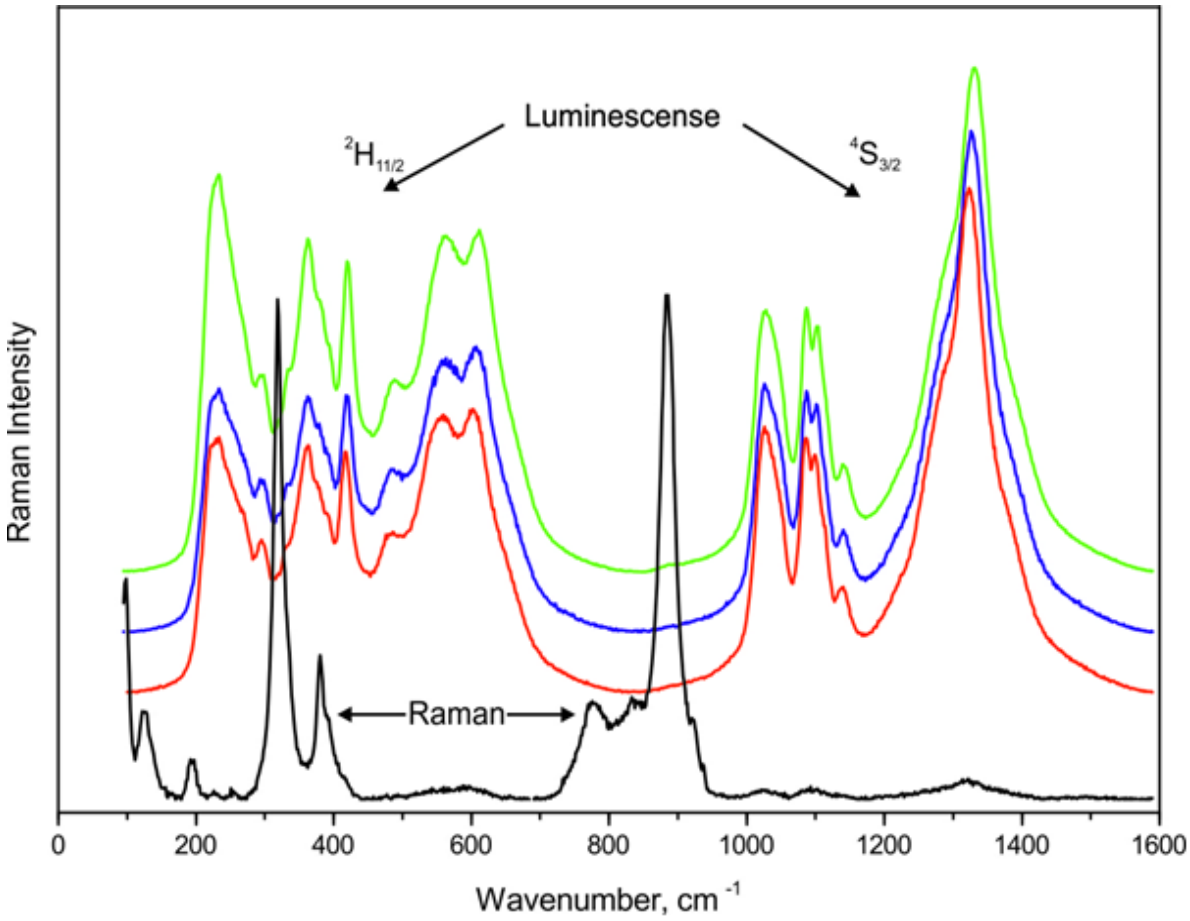

Fig. 9. Emission (Raman and luminescence) spectra of the synthesized (black) NCLM, (red) NCLM:0.2Er^{3+}, (blue) NCLM:0.1Er^{3+},0.2Yb^{3+}, and (green) NCLM:0.05Er^{3+},0.45Yb^{3+} particles excited by the 514.5-nm line of an Ar ion laser at 0.5 mW. Luminescence from $^2H_{11/2}$ and $^4S_{3/2}$ multiplets of Er^{3+} ion is indicated.

synthesized particles. The symmetry and frequencies of all observed modes in the Raman spectrum of pure NCLM in comparison with Raman of isostructural $CaMoO_4$[57,58] are presented in Table 2. The decomposition of spectral regions corresponding to the bending and stretching vibrations of MoO_4 tetrahedra is show in Fig. 10.

Table 2. Notation and wavenumber values (cm-1) of the active Raman lines in (a) NCLM, (b) NCLM:0.2Er^{3+}, (c) NCLM:0.1Er^{3+},0.2Yb^{3+} and (d) NCLM:0.05Er^{3+},0.45Yb^{3+}

Number	Symmetry type	exp.	calc.				exp.	
		(a)		(b)	(c)	(d)	$CaMoO_4$ [57,58]	$CaLa_2(MoO_4)_4$ [7]
1	A_g	885	881	907	874	895	877	906
2	B_g	829	822	849	826	841	845	828
3	E_g	777	785	804	779	798	792	762
4	B_g	390	398	420	424	430	402	393
5	E_g	380	371	378	384	388	391	377
6	B_g	332	330	328	315	328	327	333
7	A_g	318	326	348	343	347	321	317
8	E_g	255	241	257	267	272	267	251
9	B_g	228	231	219	229	229	214	
10	A_g	195	202	193	200	202	204	193
11	E_g	190?	183	186	192	196	189	
12	B_g	141	142	149	151	152	143	
13	E_g	125	127	131	134	137	111	
14	B_g	96	96	90	95	95		
15	E_g		79	80	83	85		
16	B_g		21	20	21.4	21.4		
17	E_g		18	18	18.8	19.4		
18	B_g			18	19.7	19.6		

19	E_g			16	17.2	17.7		
20	B_g				19.1	19.1		
21	E_g				16.8	17.4		

To perform the lattice dynamics (LD) simulation of investigated compounds the program package LADY was used [59]. The atomic vibration frequencies were obtained using the modified random-element-isodisplacement model [60]. Only the pair-wise interactions and bond-stretching force constants A are considered. A depends on r_{ij} and the $A(r_{ij})$ dependencies are the same for all atom pairs – $A = \lambda\exp(-r_{ij}/\rho)$, where r_{ij} is the interatomic distance, and λ and ρ are the parameters characterizing the selected pair interaction. To find model parameters, the special optimization program was written and tested for several compounds from different chemical classes [7,47,61-66]. The initial parameter values were accepted as random ones and lattice stability conditions were taken into account. The resulting model

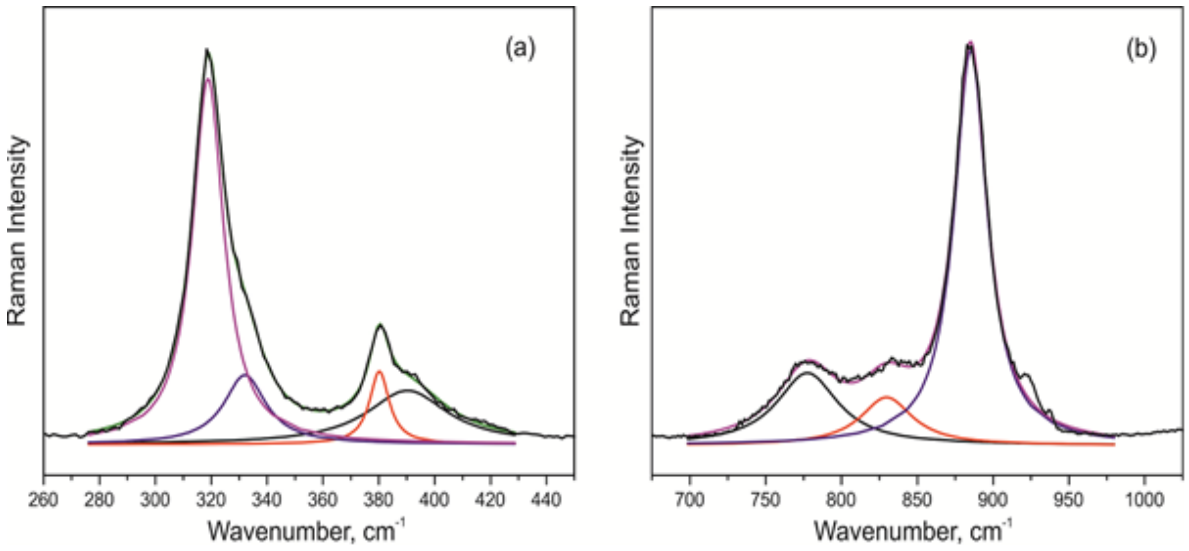

Fig. 10. The decomposition of Raman spectra of NCLM in the regions of (a) bending and (b) stretching vibrations of MoO_4 tetrahedra.

parameters were obtained by minimization of residual difference values of the simulated and experimental Raman frequencies of pure NCLM using the Fletcher–Reeves method [67]. In the case of suspension of the Fletcher–Reeves algorithm because of the incompatible model parameters, the initial model parameters were set random again. To obtain a satisfactory agreement of experimental and calculated results, O–O intramolecular interactions within the MoO_4 tetrahedral groups and O–O intermolecular interactions between neighboring MoO_4 groups should be described within the different force constants, and the cation–cation interactions can be neglected [68,69]. The model parameters obtained for pure NCLM are shown in Table 4S. The simulations of NCLM:0.2Er^{3+}, NCLM:0.1Er^{3+},0.2Yb^{3+}, NCLM:0.05Er^{3+},0.45Yb^{3+} were carried out using the same model parameters. The uniform values of Er–O, Yb–O and La–O force constants were selected. The comparison of the observed and calculated Raman modes of pure NCLM can be found in Table 2. Calculations predict noticeable shifts of Raman frequencies in doped samples; the extent of these shifts is in general agreement with the variation of Mo-O length according to the empirical formula by Hardcastle [70]. However, the Raman signals measured for Er-doped compositions can not be directly compared to the simulated results because of strong Er^{3+} luminescence, and the experimental check must be the subject of a separate study.

By the group theory analysis, 17 active Raman modes were predicted for the NCLM structure: $\Gamma_{raman} = 3A_g + 7B_g + 7E_g$; 19 active modes for NCLM:0.2Er^{3+}: $\Gamma_{raman} = 3A_g + 8B_g + 8E_g$; 21 active modes for NCLM:0.1Er^{3+},0.2Yb^{3+} and NCLM:0.05Er^{3+},0.45Yb^{3+}: $\Gamma_{raman} = 3A_g + 9B_g + 9E_g$. As can be seen from Table 2, additional modes, in comparison with pure molybdate, should be observed in the Raman spectra of Er,Y-doped compounds in the range below 80 cm^{-1}. The most intensive band of the NCLM Raman spectrum found at 884 cm^{-1} corresponds to the ν_1 symmetric stretching vibration of the MoO_4 group. The lines at 829 and 777 cm^{-1} are related to the ν_3 antisymmetric stretching vibrations. The bending ν_2 and ν_4

vibrations are situated in the wavenumber region of 300–400 cm^{-1}. The shape of the observed normal vibration modes of tetrahedral MoO_4 groups was considered in Ref. 71. The translation and rotational vibrations of MoO_4 are in the region of 150–260 cm^{-1}. The big cation vibrations are below 150 cm^{-1}. As it can be seen from the comparison of Raman spectra of pure NCLM and $CaLa_2(MoO_4)_4$[7] shown in Fig. 5S, the positions of the bands corresponding to the symmetric stretching of MoO_4 are a little different in these crystals. In this case, according to the LD model presented above, Mo-O bonds should have different lengths in these molybdates and this is confirmed by structural results (Table 2S). As to Raman spectra of the doped samples recorded under the excitation at 514.5-nm, the Raman lines are superimposed by strong Er^{3+} luminescence lines. To consider the vibrational spectra of the these samples, it is topical to use the excitation source with a drastically longer wavelength that should avoid the excitation of Er^{3+} ion optical transitions.

4. Conclusions

The triple molybdate NCLM:xEr^{3+},yYb^{3+} phosphors were successfully synthesized by microwave sol-gel method. Well-crystallized particles formed after heat-treatment at 900°C for 16 h showed a fine and homogeneous morphology with particle sizes of 2-3 μm. Under excitation at 980 nm, the UC doped particles exhibited a strong 525-nm emission band and weak 550-nm emission band in the green region, which correspond to the $^2H_{11/2} \rightarrow {}^4I_{15/2}$ and $^4S_{3/2} \rightarrow {}^4I_{15/2}$ transitions, and a very weak 655-nm emission band in the red region, which corresponds to the $^4F_{9/2} \rightarrow {}^4I_{15/2}$ transition. The preferable Yb^{3+}:Er^{3+} ratio of 9:1 is controlled by the concentration quenching effect in Er^{3+} ions. The calculated slope value *n* indicated the slopes of $n = 1.70$ and 1.68 for the green emission at 525 and 550 nm, respectively, and $n = 1.56$ for the red emission at 655 nm. The calculated chromaticity coordinates of the NCLM:xEr^{3+},yYb^{3+} phosphors are correspondent to the yellowish-green sector in CIE

diagram. These results demonstrate high emitting efficiency NCLM:xEr^{3+},yYb^{3+} UC phosphors and new materials from this crystal family can be considered potentially as active components in new optoelectronic devices and in the field of luminescent imaging.

Acknowledgements

This research was supported by the Basic Science Research Program through the National Research Foundation of Korea (NRF) funded by the Ministry of Education (2015-058813), by the Russian Foundation for Basic Research (15-52-53080) and by Project №0358-2015-0012 of SB RAS Program №II.2P. ASO and VVA are partially supported by the Ministry of Education and Science of the Russian Federation.

References

1. M.V. DaCosta, S. Doughan, Y. Han, U.J. Krull, Lanthanide upconversion nanoparticles and applications in bioassays and bioimaging: A review, Anal. Chim. Acta, 832 (2014) 1-33.
2. Y.J. Chen, H.M. Zhu, Y.F. Lin, X.H. Gong, Z.D. Luo, Y.D. Huang, Efficient diode-pumped continuous-wave monolithic 1.9 μm micro-laser based on Tm^{3+}:$BaGd_2(MoO_4)_4$ cleaved plate, Opt. Mat. 35 (2013) 1422-1425.
3. C. Zhang, L.D. Sun, Y.W. Zhang, C.H. Yan, Rare earth upconversion nanophosphors: synthesis, functionalization and application as biolabels and energy transfer donors, J. Rare Earths 28 (2010) 807-819.
4. V.V. Atuchin, O.D. Chimitova, T.A. Gavrilova, M.S. Molokeev, S.-J. Kim, N.V. Surovtsev, B.G. Bazarov, Synthesis. Structural and vibrational properties of microcrystalline $RbNd(MoO_4)_3$, J. Cryst. Growth 318 (2011) 683-686.

5. V.A. Morozov, A. Bertha, K.W. Meert, S. Van Rompaey, D. Batuk, G.T. Martinez, S. Van Aert, P.F. Smet, M.V. Raskina, D. Poelman, A.M. Abakumov, J. Hadermann, Incommensurate Modulation and Luminescence in the $CaGd_{2(1-x)}Eu_{2x}(MoO_4)_{4(1-y)}(WO_4)_{4y}(0 \le x \le 1, 0 \le y \le 1)$ Red Phosphors, Chem. Mater. 25 (2013) 4387-4395.
6. P.L. Shi, Z.G. Xia, M.S. Molokeev, V.V. Atuchin, Crystal chemistry and luminescence properties of red-emitting $CsGd_{1-x}Eu_x(MoO_4)_2$ solid-solution phosphors, Dalton Trans. 43 (2014) 9669-9676.
7. C.S. Lim, A. Aleksandrovsky, M. Molokeev, A. Oreshonkov, V. Atuchin, The modulated structure and frequency upconversion properties of $CaLa_2(MoO_4)_4:Ho^{3+}/Yb^{3+}$ phosphors prepared by microwave synthesis, Phys. Chem. Chem. Phys. 17 (2015) 19278- 19287.
8. V.V. Atuchin, A.S. Aleksandrovsky, O.D. Chimitova, C.-P. Diao, T.A. Gavrilova, V.G. Kesler, M.S. Molokeev, A.S. Krylov, B.G. Bazarov, J.G. Bazarova, Z.S. Lin, Electronic structure of β-$RbSm(MoO_4)_2$ and chemical bonding in molybdates, Dalton Trans. 44 (2015) 1805-1815.
9. C.S. Lim, Highly modulated structure and upconversion photoluminescence properties of $PbGd_2(MoO_4)_4:Er^{3+}/Yb^{3+}$, Mater. Res. Bull. 75 (2016) 211-216.
10. Chimitova, V.V. Atuchin, B.G. Bazarov, M.S. Molokeev, Z.G. Bazarova, The formation and structural parameters of new double molybdates $RbLn(MoO_4)_2$ (Ln = Pr, Nd, Sm, Eu), Proc. SPIE 8771 (2013) 87711A.
11. C.F. Guo, H.K. Yang, J.-H. Jeong, Preparation and luminescent properties of phosphor $MGd_2(MoO_4)_4$: Eu^{3+} (M = Ca, Sr and Ba), J. Lumin. 130 (2010) 1390-1393.
12. J.Y. Sun, Y.J. Lan, Z.G. Xia, H.Y. Du, Sol–gel synthesis and green upconversion luminescence in $BaGd_2(MoO_4)_4:Yb^{3+},Er^{3+}$ phosphors, Opt. Mater. 33 (2011) 576-581.

13. J.S. Liao, D. Zhou, B. Yang, R.Q. Liu, Q. Zhang, Q.H. Zhou, Sol–gel preparation and photoluminescence properties of $CaLa_2(MoO_4)_4:Eu^{3+}$ phosphors, J. Lumin. 134 (2013) 533-538.
14. F.R. Chen, Z.G. Xia, M.S. Molokeev, X.P. Jing, Effects of composition modulation on the luminescence properties of Eu^{3+} doped $Li_{1-x}Ag_xLu(MoO_4)_2$ solid-solution phosphors, Dalton Trans. 44 (2015) 18078-18089.
15. C.S. Lim, Preparation of $CaLa_2(MoO_4)_4:Er^{3+}/Yb^{3+}$ phosphors via the microwave-modified sol-gel route and the upconversion of their photoluminescence properties, Mater. Res. Bull. 60 (2014) 537-542.
16. C.S. Lim, Upconversion photoluminescence properties of $SrY_2(MoO_4)_4:Er^{3+}/Yb^{3+}$ phosphors synthesized by a cyclic microwave-modified sol-gel method, Inf. Phys. Tech. 67 (2014) 371-376.
17. J.Y. Sun, W. Zhang, W.H. Zhang, H.Y. Du, Synthesis and two-color emission properties of $BaGd_2(MoO_4)_4:Eu^{3+},Er^{3+},Yb^{3+}$ phosphors, Mater. Res. Bull. 47 (2012) 786-789.
18. J.F. Tang, C.H. Cheng, Y.J. Chen, Y.D. Huang, Yellow–green upconversion photoluminescence in Yb^{3+}, Ho^{3+} co-doped $NaLa(MoO_4)_2$ phosphor, J. Alloys Compd. 609 (2014) 268-273.
19. W.T. Zhang, J.F. Li, Y.L. Wang, J.P. Long, K.H. Qiu, Synthesis and luminescence properties of $NaLa(MoO_4)_{2-x}AG_x:Eu^{3+}$ (AG = SO_4^{2-}, BO_3^{3-}) red phosphors for white light emitting diodes, J. Alloys Compd. 635 (2015) 16-20.
20. F.W. Mo, L. Zhou, Q. pang, F.Z. Gong, Z.J. Liang, Potential red-emitting $NaGd(MO_4)_2:R$ (M = W, Mo, R = Eu^{3+}, Sm^{3+}, Bi^{3+}) phosphors for white light emitting diodes applications, Ceram. Inter. 38, (2012) 6289-6294.

21. G.H. Li, S. Lan, L.L. Li, M.M. Li, W.W. Bao, H.F. Zou, X.C. Xu, S.C. Gan, Tunable luminescence properties of $NaLa(MoO_4)_2:Ce^{3+},Tb^{3+}$ phosphors for near UV-excited white light-emitting-diodes, J. Alloys Compd. 513 (2012) 145-149.
22. J.S. Liao, H.Z. Huang, H.Y. You, X. Qiu, Y. Li, B. Qui, H.-R. Wen, Photoluminescence properties of $NaGd(MoO_4)_2:Eu^{3+}$ nanophosphors prepared by sol–gel method, Mater. Res. Bull. 45 (2010) 1145-1149.
23. F.-B. Cao, L.-S. Li, Y.-W. Tian, X.-R. Wu, Sol–gel synthesis of red-emitting $[Na_{0.6}La_{0.8-x}Eu_x]_2(MoO_4)_3$ phosphors and improvement of its luminescent properties by the co-doping method, Opt. Laser Tech. 55 (2014) 6-10.
24. G.M. Kuz'micheva, D.A. Lis, K.A. Subbotin, V.B. Rybakov, E.V. Zharikov, Growth and structural X-ray investigations of scheelite-like single crystals Er, Ce:$NaLa(MoO_4)_2$ and Yb:$NaGd(WO_4)_2$, J. Crys. Growth 275 (2005) e1835- e1842.
25. X.A. Lu, Z.N. You, J.F. Li, Z.J. Zhu, G.H. Jia, B.C. Wu, C.Y. Tu, Optical absorption and spectroscopic characteristics of Tm^{3+} ions doped $NaY(MoO_4)_2$ crystal, J. Alloys Compd. 458 (2008) 462-466.
26. X.Z. Li, Z.B. Lin, L.Z. Zhang, G.F. Wang, Growth, thermal and spectral properties of Nd^{3+}-doped $NaGd(MoO_4)_2$ crystal, J. Crys. Growth 290 (2006) 670-673.
27. Y.K.Voron'ko, K.A. Subbotin, V.E. Shukshin, D.A. Lis, S.N. Ushakov, A.V. Popov, E.V. Zharikov, Growth and spectroscopic investigations of Yb^{3+}-doped $NaGd(MoO_4)_2$ and $NaLa(MoO_4)_2$ - new promising laser crystals, Opt. Mater. 29 (2009) 246-252.
28. H. Lin, X.H. Yan, X.F. Wang, Controllable synthesis and down-conversion properties of flower-like $NaY(MoO_4)_2$ microcrystals via polyvinylpyrrolidone-mediated, J. Solid State. Chem. 204 (2013) 266-271.

29. G.H. Li, L.L. Li, M.M. Li, W.W. Bao, Y.H. Song, S.C. Gan, H.F. Zou, X.C. Xu, Hydrothermal synthesis and luminescent properties of $NaLa(MoO_4)_2:Eu^{3+},Tb^{3+}$ phosphors, J. Alloys Compd. 550 (2013) 1-8.

30. Y. Huang, L.Q. Zhou, L. Yang, Z.W. Tang, Self-assembled 3D flower-like $NaY(MoO_4)_2:Eu^{3+}$ microarchitectures: Hydrothermal synthesis, formation mechanism and luminescence properties, Opt. Mater. 33 (2011)777-782.

31. L.L. Li, W.W. Zi, G.H. Li, S. Lan, G.J. Ji, S.C. Gan, H.F. Zou, X.C. Xu, Hydrothermal synthesis and luminescent properties of $NaLa(MoO_4)_2:Dy^{3+}$ phosphor, J. Solid State Chem. 191 (2012) 175-180.

32. Y. Tian, B.J. Chen, B.N. Tian, J.S. Sun, X.P. Li, J.S. Zhang, L.H. Cheng, H.Y. Zhong, H. Zhong, Q.G. Meng, R.N. Hua, Ionic liquid-assisted hydrothermal synthesis of dendrite-like $NaY(MoO_4)_2:Tb^{3+}$ phosphor, Physica B 407 (2012) 2556-2559.

33. J.C. Zhang, X.F. Wang, X.H. Zhang, X.D. Zhao, X.Y. Liu, L.P. Peng, Microwave synthesis of $NaLa(MoO_4)_2$ microcrystals and their near-infrared luminescent properties with lanthanide ion doping (Er^{3+}, Nd^{3+}, Yb^{3+}), Inorg. Chem. Commun. 14 (2011) 1723-1727.

34. S.W. Park, B.K. Moon, B.C. Choi, J.H. Jeong, J.S. Bae, K.H. Kim, Red photoluminescence of pulsed laser deposited $Eu:NaY(MoO_4)_2$ thin film phosphors on sapphire substrates, Curr. Appl. Phys. 12 (2012) S150-S155.

35. K.I. Rybakov, E.A. Olevsky, E.V. Krikun, Microwave sintering: Fundamentals and modeling, J. Am. Ceram. Soc. 96 (2013) 1003-1020.

36. H.J. Kitchen, S.R. Vallance, J.I. Kennedy, N. Tapia-Ruiz, L. Carassiti, A. Harrison, A.G. Whittaker, T.D. Drysdale, S.W. Kingman, D.H. Gregory, Modern microwave methods in solid-state inorganic materials chemistry: From fundamentals to manufacturing, Chem. Rev. 114 (2014) 1170-1206.

37. C.S. Lim, Cyclic MAM synthesis and upconversion photoluminescence properties of $CaMoO_4:Er^{3+}/Yb^{3+}$ particles, Mater. Res. Bull. 47 (2012) 4220-4225.
38. C.S. Lim, Preparation of $PbLa_2(MoO_4)_2:Er^{3+}/Yb^{3+}$ particles via microwave sol-gel route and upconversion photoluminescence properties, Ceram. Inter. 41 (2015) 12464-12470.
39. C.S. Lim, A. Aleksandrovsky, M. Molokeev, A. Oreshonkov, V. Atuchin, Microwave sol-gel synthesis of $CaGd_2(MoO_4)_2:Er^{3+}/Yb^{3+}$ phosphors and their upconversion photoluminescence properties, J. Am. Ceram. Soc. 98 (2015) 3223-3230.
40. Bruker AXS TOPAS V4: General profile and structure analysis software for powder diffraction data. – User's Manual. Bruker AXS, Karlsruhe, Germany, 2008.
41. R.M. Hazen, L.W. Finger, J.W.E. Mariathasan, High-pressure crystal chemistry of scheelite-type tungstates and molybdates, J. Phys. Chem. Solids 46 (1985) 253-263.
42. S.B. Stevens, C.A. Morrison, T.H. Allik, A.L. Rheingold, B.S. Haggerty, $NaLa(MoO_4)_2$ as a laser host material, Phys. Rev. B 43 (1991) 7386-7394.
43. http://www.iucr.org/__data/iucr/cifdic_html/1/cif_core.dic/Cchemical_formula.html.
44. R.D. Shannon, Revised effective ionic radii and systematic studies of interatomic distances in halides and chalcogenides, Acta Cryst. A 32 (1976) 751-767.
45. V.V. Atuchin, V.G. Grossman, S.V. Adichtchev, N.V. Surovtsev, T.A. Gavrilova, B.G. Bazarov, Structural and vibrational properties of microcrystalline $TlM(MoO_4)_2$ (M = Nd, Pr) molybdates, Opt. Mater. 34 (2012) 812-816.
46. V.V. Atuchin, A.S. Aleksandrovsky, O.D. Chimitova, A.S. Krylov, M.S. Molokeev, B.G. Bazarov, J.G. Bazarova, Zhiguo Xia, Synthesis and spectroscopic properties of multiferroic β'-$Tb_2(MoO_4)_3$, Opt. Mater. 36 (2014) 1631-1635.
47. V.V. Atuchin, A.S. Aleksandrovsky, O.D. Chimitova, T.A. Gavrilova, A.S. Krylov, M.S. Molokeev, A.S. Oreshonkov, B.G. Bazarov, J.G. Bazarova, J. Phys. Chem. Synthesis and spectroscopic properties of monoclinic α-$Eu_2(MoO_4)_3$, C 118 (2014) 15404-15411.

48. V.V. Atuchin, T.A. Gavrilova, J.-C. Grivel, Electronic structure of layered titanate $Nd_2Ti_2O_7$, Surf. Sci. 602 (2008) 3095-3099.

49. V.V. Atuchin, S.V. Adichtchev, B.G. Bazarov, Zh.G. Bazarova, T.A. Gavrilova, V.G. Grossman, V.G. Kesler, G.S. Meng, Z.S. Lin, N.V. Surovtsev, Electronic structure and vibrational properties of $KRbAl_2B_2O_7$, Mater. Res. Bull. 48 (2013) 929-934.

50. V. Atuchin, L. Zhu, S. H. Lee, D. H. Kim, C. S. Lim, Microwave-assisted solvothermal synthesis of $Sr_3V_2O_8$ nanoparticles and their spectroscopic properties, Asian J. Chem. 26 (5) (2014) 1290-1292.

51. F. Auzel, G. Baldacchini, L. Laversenne, G. Boulon, Radiation trapping and self-quenching analysis in Yb^{3+}, Er^{3+}, and Ho^{3+} doped Y_2O_3, Opt. Mater. 24 (2003) 103-109.

52. M. Pollnau, D.R. Gamelin, S.R. Lüthi, H.U. Güdel, Power dependece of upconversion luminescence in lanthanide and transition-metal-ion systems, Phys. Rev. B 61 (2000) 3337-3346.

53. H.Y. Du, Y.J. Lan, Z.G. Xia, J.Y. Sun, Synthesis and upconversion luminescence properties of Yb^{3+}/Er^{3+} codoped $BaGd_2(MoO_4)_4$ powder, Mater. Res. Bull. 44 (2009) 1660-1662.

54. B. Li, B. Joshi, Y.K. Kshetri, R. Adhikari, R.N. Gracia, S.W. Lee, Upconversion luminescence properties of Er^{3+}/Yb^{3+} in transparent a-Sialon ceramics, Opt. Mater. 39 (2015) 239-246.

55. J.H. Chung, J.-I. Lee, S.-L. Ryu, J.H. Ryu, Visible green upconversion luminescence of $Er^{3+}/Yb^{3+}/Li^{+}$ co-doped $CaWO_4$ particles, Ceram. Int. 39 (2013) S369-S372.

56. J. Castañeda, M.A. Meneses-Nava, O. Barbosa-García, E. de la Rosa-Cruz, J.F. Mosiño, The red emission in two and three steps up-conversion process in a doped erbium SiO_2–TiO_2 sol–gel powder, J. Lumin. 102-103 (2003) 504-509.

57. E. Sarantopoulou, C. Raptis, S. Ves, D. Christofilos and G. A. Kourouklis, Temperature and pressure dependence of Raman-active phonons of $CaMoO_4$: an anharmonicity study, J. Phys.: Condens. Matter 14 (2002) 8925–8938.

58. P.G. Zverev, Vibronic relaxation of Raman modes in $CaMoO_4$ and $PbMoO_4$ molecular ionic crystals, Phys. Stat. Sol. C 1 (2004) 3101–3105.

59. M.B. Smirnov, V.Yu. Kazimirov. LADY: software for lattice dynamics simulations. (JINR communications), E 14-2001-159 (2001).

60. I.F. Chang, S.S. Mitra, Application of a modified random-element-isodisplacement model to long-wavelength optic phonons of mixed crystals, Phys. Rev. 172 (1968) 924 – 933.

61. A.N. Vtyurin, A.S. Krylov, S.N. Krylova, S.V. Goryainov, V.N. Voronov, A.S. Oreshonkov, Hydrostatic pressure-induced phase transitions in Rb_2KInF_6 and Rb_2KScF_6 crystals: Raman spectra and lattice dynamics simulations, Ferroelectrics 440 (2012) 100-104.

62. Y.V. Gerasimova, A.S. Oreshonkov, A.N. Vtyurin, A.A. Ivanenko, L.I. Isaenko, A.A. Ershov, E.I. Pogoreltsev, Infrared absorption investigation of the role of octahedral groups upon the phase transition in the $Rb_2KMoO_3F_3$ crystal, Phys. Solid State 55 (2013) 2331-2334.

63. A.S. Krylov, A.N. Vtyurin, A.S. Oreshonkov, V.N. Voronov, S.N. Krylova, Structural transformations in a single-crystal Rb_2NaYF_6: Raman scattering study, J. Raman Spectr. 44 (2013) 763-769.

64. Z.G. Xia, M.S. Molokeev, A.S. Oreshonkov, V.V. Atuchin, R.-S. Liu, C. Dong, Crystal and local structure refinement in $Ca_2Al_3O_6F$ explored by X-ray diffraction and Raman spectroscopy, Phys. Chem. Chem. Phys. 16 (2014) 5952-5957.

65. A.A. Savina, V.V. Atuchin, S.F. Solodovnikov, Z.A. Solodovnikova, A.S. Krylov, E.A. Maximovskiy, M.S. Molokeev, A.S Oreshonkov, A.M. Pugachev, E.G. Khaikina, Synthesis, structural and spectroscopic properties of acentric triple molybdate $Cs_2NaBi(MoO_4)_3$, J. Solid State Chem. 225 (2015) 53–58.
66. C.S. Lim, A. Aleksandrovsky, M. Molokeev, A. Oreshonkov, V. Atuchin, Microwave sol-gel synthesis and upconversion photoluminescence properties of $CaGd_2(WO_4)_4:Er^{3+}/Yb^{3+}$ phosphors with incommensurately modulated structure, J. Solid State Chem. 228 (2015) 160-166.
67. R. Fletcher, Practical Methods of Optimization, 2nd edn, Wiley, Chichester etc., 1987.
68. Senyshyn, H. Kraus, V. B. Mikhailik, and V. Yakovyna, Lattice dynamics and thermal properties of $CaWO_4$, Phys. Rev. B 70, (2004) 214306.
69. Senyshyn, H. Kraus, V. B. Mikhailik, L. Vasylechko, and M. Knapp, Thermal properties of $CaMoO_4$: Lattice dynamics and synchrotron powder diffraction studies, Phys. Rev. B 73, (2006) 014104.
70. F. D. Hardcastle, I. E. Wachs, Determination of molybdenum-oxygen bond distances and bond orders by Raman spectroscopy, J. Raman Spectr. 21 (1990) 683-691.
71. K. Nakamoto, Infrared and Raman Spectra of Inorganic and Coordination Compounds. 6th ed. Wiley, New York etc., 2009.